

Discovery of Associated Absorption Lines in an X-Ray Warm Absorber: *HST-FOS* Observations of MR2251–178¹

Eric M. Monier² and Smita Mathur³

Department of Astronomy, The Ohio State University

140 W. 18th Ave., Columbus, OH 43204

and

Belinda Wilkes and Martin Elvis

Harvard-Smithsonian Center for Astrophysics

60 Garden Street, Cambridge, MA 02138

ABSTRACT

The presence of a “warm absorber” was first suggested to explain spectral variability in an X-ray spectrum of the radio-quiet QSO MR2251–178. A unified picture, in which X-ray warm absorbers and “intrinsic” UV absorbers are the same, offers the opportunity to probe the nuclear environment of active galactic nuclei. To test this scenario and understand the physical properties of the absorber, we obtained a UV spectrum of MR2251–178 with the Faint Object Spectrograph (FOS) onboard the *Hubble Space Telescope (HST)*. The *HST* spectrum clearly shows absorption due to Ly α , N V and C IV, blueshifted by 300 km s⁻¹ from the emission redshift of the QSO. The rarity of both X-ray and UV absorbers in radio-quiet QSOs suggests these absorbers are physically related, if not identical. Assuming the unified scenario, we place constraints on the physical parameters of the absorber and conclude the mass outflow rate is essentially the same as the accretion rate in MR2251–178.

Subject headings: quasars: absorption lines — quasars: individual (MR2251–178)
– ultraviolet: galaxies

¹Based on Observations with the NASA/ESA *Hubble Space Telescope*, obtained at the Space Telescope Science Institute, which is operated by AURA, Inc., under NASA contract NAS 5-26555.

²monier@astronomy.ohio-state.edu

³smita@astronomy.ohio-state.edu

1. Introduction

Absorption due to O VII and O VIII in the X-ray and O VI in the UV can in some cases be modeled by a single UV/X-ray absorber (Mathur 1994; Mathur, Wilkes, & Elvis 1998), offering a unique way to determine the physical conditions of the absorbing material in active galactic nuclei (AGNs). As more X-ray/UV absorbers have been found (e.g., Mathur 1994; Mathur, Elvis, & Wilkes 1995; Mathur, Elvis, & Singh 1995; Mathur, Wilkes, & Aldcroft 1997; Shields & Hamann 1997; Mathur et al. 1998; Hamann, Netzer, & Shields 2000) it has become clear these share common characteristics. Though not all of these absorbers can be readily modeled by a single zone, all are composed of highly ionized, low density, high column density, outflowing gas sitting outside the broad emission line region (BELR). The X-ray/UV absorbers are therefore an important nuclear component of AGNs, representing a wind or outflow carrying away significant kinetic energy at a mass-loss rate comparable to the accretion rate needed to power the AGN (Mathur et al. 1995). The properties of these absorbers can be invoked in AGN models developed to explain such outflows (see Elvis 2000 and references therein), and will aid in expanding such models into a wider unification scenario (Elvis 2000).

It remains to be determined how common X-ray/UV absorbers are. In a sample of eight Seyfert galaxies, Crenshaw et al. (1999) found six of them showed both UV and X-ray absorption, strengthening the UV/X-ray connection. The question remains whether X-ray absorbers are physically related to UV absorbers in all AGN (two of the Seyferts of the Crenshaw et al. sample were not X-ray warm absorbers and showed no UV absorption), or, if not, in what fraction of cases does the unified model apply. To help answer these questions, we initiated an *HST* program to search for UV absorption in two radio-quiet QSOs with known X-ray warm absorbers.

Mathur et al. (1998) reported UV absorption in the first of these objects, PG1114+445. Here we present the detection of UV absorption in our second candidate, MR2251–178, a low-redshift ($z_{em} = 0.0640$) radio-quiet QSO. In addition to being the first X-ray selected QSO (Ricker et al. 1978), MR2251–178 was the object for which Halpern (1984) originally suggested the presence of partially ionized, optically thin material: the X-ray warm absorber.

In §2 we describe the *HST* observations and the analysis of the UV absorption lines. Section 3 relates the UV absorption to the X-ray absorption seen in ASCA data analyzed by Reynolds (1997) and presents some simple physical quantities based on the assumption that the UV and X-ray absorbers are the same. We present our conclusions in §4.

2. The *HST* spectra

On 1996 February 2, MR2251–178 was observed using three gratings of the *Faint Object Spectrograph* onboard *HST*. The target was centered in the 1" circular aperture through a four step peak-up sequence to ensure a pointing accuracy of 0".12. Two exposures totalling 5740s were obtained using the G130H grating and blue side of the detector. The exposures using the red side and the G190H and G270H gratings were 1730s and 300s, respectively.

The data were reduced using the standard pipeline processing and calibration files, and the individual G130H spectra were combined. The final spectra are shown in Figure 1. Absorption lines of Ly α , C IV and N V can be clearly seen, as predicted from the X-ray/UV models. The strong absorption lines of Ly α and C IV are superposed on the emission lines of Ly α and C IV. Weaker absorption due to the N V doublet is seen against the continuum; no measurable N V emission is present. The spectra do not show absorption due to low-ionization Mg II indicating the X-ray absorber is highly ionized.

There is an inherent uncertainty involved in measuring an absorption line lying on top of a broad emission line profile because the unabsorbed shape of the emission line is unknown. We therefore used two methods to measure the line equivalent widths (EWs) as in Mathur et al. (1998). We made an initial measurement using the IRAF SPLOT task to fit Gaussians across the absorption in the emission line profiles. A single Gaussian was used for Ly α and N V lines, and the C IV doublet is deblended into two Gaussians. Results for the EWs and FWHMs are listed in Table 1. We estimate the errors on the EWs for Ly α and C IV to be $\sim 40\%$. The continuum is more readily determined on either side of the N V lines, hence the error on the SPLOT measurement is estimated at $\sim 10\%$. The C IV and N V doublet ratios are both ≈ 1.7 , so the doublets may be partially saturated, though not as severely as in PG1114+445. Higher resolution spectra would be needed to address the degree of saturation. Also, though it is probable the individual lines will break into multiple components at higher resolution (Ly α in fact has two components; see §3.1), we treat them as single lines here.

To obtain a more accurate estimate of the absorption line EWs, we used the SPECFIT (Kriss 1994) task under STSDAS to simultaneously fit the underlying continuum and the emission and absorption line profiles. The continuum was characterized by a simple power law, the emission lines were fit with multiple Gaussians, and each absorption line was fit with a single Gaussian. First, the power-law continuum was fit to featureless parts of the spectrum on either side of the emission lines and the absorption to be measured. The parameters of the power-law continuum – the slope and the normalization – were then fixed in subsequent fits. The parameters of the Gaussians used to fit the emission lines (flux, centroid, FWHM and skew) and the absorption lines (flux, centroid and FWHM) were allowed to vary freely. The fits to the Ly α , N V and C IV emission/absorption profiles are shown in Figure 2, and

the corresponding EW and FWHM of the absorption fits are given in Table 1. The results of the SPLOT and SPECFIT methods are qualitatively similar, although the SPECFIT values are systematically larger due to the higher continuum provided by fitting the emission lines. These differences are unimportant to the discussion.

The observed FWHM of the absorption lines is 1.3 - 3.0 Å ($>300 \text{ km s}^{-1}$) with SPLOT and 1.4 - 3.3 Å ($>320 \text{ km s}^{-1}$) with SPECFIT. For each ion the total absorption is likely resolved given the $\approx 230 \text{ km s}^{-1}$ resolution of FOS, so the absorber is dispersed in velocity space. In a higher resolution spectrum, however, the absorption lines may split into multiple components. The average absorption redshift for the five lines is $\langle z \rangle = 0.063$, blueshifted by 300 km s^{-1} from the QSO emission redshift of $z_{em} = 0.0640$ (Bergeron et al. 1983). We expect that O VI absorption is also present, but it lies below the blue cutoff of the G130H grating at the redshift of MR2251–178.

MR2251–178 was also observed in 1998 Dec by J. Stocke with HST-STIS over the wavelength range 1250–1300Å. The Ly α absorption line breaks into a broad component and a narrow component at the $\approx 12 \text{ km s}^{-1}$ resolution of the STIS G140M grating. Figure 3 shows the Ly α region and a fit to the absorption profile produced with SPECFIT as described previously. The resulting line centers, EWs and FWHMs of the two components are listed in Table 1.

3. The X-Ray/UV Absorber

High-ionization UV absorption lines due to Ly α , N V, and C IV are seen in the *HST* spectrum of MR2251–178, as predicted by UV/X-ray models. Mathur et al. (1998) estimate the chance probability that a radio-quiet QSO will have both associated UV and X-ray ionized absorption to be $\sim 1.7 \times 10^{-3}$. This strongly suggests the two absorption systems are physically related.

3.1. Physical Properties of the Ionized Gas

To explore the possibility that the UV and X-ray absorption lines arise in the same component of the nuclear material of the AGN, we need to compare the properties of the UV and X-ray absorbers.

We took the measurements of the X-ray absorber in MR2251–178 from the analysis of ASCA data (obtained 6 Nov 1993) by Reynolds (1997; Komossa 2001 obtains a similar result using ROSAT data from the same epoch). The total equivalent hydrogen column density of

the X-ray absorber is $N_{\text{H}} = 5 \times 10^{21}$ atoms cm^{-2} , determined by fitting the warm absorber with a one-zone model using the CLOUDY photoionization code (Ferland 1996). Reynolds constrained the optical depths of the O VII/O VIII edges in a simple two-edge model with a power-law continuum ($\alpha = 1.73$). We used these values as an input to CLOUDY to derive the column densities of the UV ions seen in absorption in the *HST* data. The standard “Table AGN” (Mathews & Ferland 1987) continuum (with a resulting ionization parameter of $U = 1.0$)⁴ was used with the assumption of solar abundances. The shape of the observed UV continuum of MR2251–178 (Figure 1) is consistent with that in “Table AGN.” Table 1 lists the CLOUDY predictions for the ionic column densities of H I, N V, and C IV, as derived from the X-ray data.

To compare these predictions to what is observed in the UV, it is necessary to convert the equivalent widths to column densities. As discussed in §2, the lines may be somewhat saturated, thus the column densities can be calculated only if the velocity dispersion parameter (b parameter) of the lines is known. If the lines are resolved, then $b \approx 450$ km s^{-1} [$b = \text{FWHM}/(4\ln 2)^{1/2}$; the FWHM is given in Table 1] for Ly α and $\approx 200 - 270$ km s^{-1} for C IV and N V. The X-ray prediction for the column density of hydrogen, $N_{\text{HI}} = 8 \times 10^{14}$ cm^{-2} , is therefore about a factor of 2 larger than the minimum value measured in the FOS data ($N_{\text{HI}} \approx 4 \times 10^{14}$ cm^{-2}). Agreement between the UV and X-ray values is achieved for $b \approx 200$ km s^{-1} , implying the line breaks into at least two components at higher resolution, as is shown in the STIS data (§2).⁵ A curve-of-growth analysis using the new b -values (~ 65 and ~ 280 km s^{-1}) results in a combined total Ly α column density of $\sim 7 \times 10^{14}$, in good agreement with the X-ray prediction for H I.

The X-ray predicted values for the N V and C IV are smaller than those calculated from the UV equivalent width measurements. For N V, the X-ray prediction is $N_{\text{NV}} = 1.6 \times 10^{14}$ cm^{-2} , while the UV equivalent width measurement gives $N_{\text{HI}} = 8 \times 10^{14}$ cm^{-2} , assuming the lines are resolved. Similarly for C IV, the X-ray prediction of $N_{\text{CIV}} = 1.6 \times 10^{13}$ cm^{-2} is more than an order of magnitude smaller than the UV measurement of $N_{\text{CIV}} \geq 7 \times 10^{14}$ cm^{-2} . The X-ray predictions for N_{NV} and especially N_{CIV} lie on the linear part of the curve of growth. If the UV and X-ray absorbers are the same, we predict these absorbers should break into multiple components – each with lower b – in UV data of higher resolution, leading to values in closer agreement with the X-ray predictions. Kinematically complex UV absorption lines have already been seen in high-resolution data of Mrk 509 (Crenshaw, Bogges & Wu 1995),

⁴ U is defined as the dimensionless ratio of ionizing photon to hydrogen number density.

⁵A weak feature at ≈ 1295.5 Å may also be Ly α redshifted relative to the quasar, as has been observed in C IV lines of NGC 5548 (Mathur, Elvis, & Wilkes 1999); this feature would not contribute significantly to N_{HI} .

NGC 4151 (Weymann et al. 1997), NGC 3516 (Kriss et al. 1996, Crenshaw et al. 1999), and NGC 5548 (Mathur et al. 1999; Crenshaw & Kraemer 1999).

Also, note the column densities derived here from the X-ray data are based on the Table AGN continuum. The shape of the actual MR2251–178 continuum in the unobserved EUV region may greatly affect the predicted column densities (Mathur et al. 1995). A better match between the observed & predicted values may be obtained if the spectral energy distribution of MR2251–178 has a different shape. In any case, the X-ray absorber is a large contributor to the absorption measured for C IV and N V in the UV, providing support for the idea that the UV and X-ray absorption is occurring in the same material.

3.2. Variability

Halpern (1984) found that the warm absorber in MR2251–178 was highly variable. ASCA data of MR2251–178 obtained in 1996 – near the epoch of the HST-FOS data – show a decrease in X-ray intensity from $\log \xi = 1.35$ in 1993 to $\log \xi = 0.96$ in 1996 (Otani, Kii, & Miya 1998), where ξ is an ionization parameter defined as $\xi \equiv L/nR^2$. If the ionization parameter U varied similarly, then in 1996 $U = 0.61$ and the X-ray-predicted column densities would be $N_{\text{CIV}} = 3.9 \times 10^{14} \text{ cm}^{-2}$ and $N_{\text{NV}} = 2.1 \times 10^{15} \text{ cm}^{-2}$, closer to the values measured in the UV data. In this case, N_{HI} grows to $3.4 \times 10^{15} \text{ cm}^{-2}$.

3.3. Physical Implications

As noted, the UV absorption indicates the material is flowing outward from the UV/X-ray absorber at $\approx 300 \text{ km s}^{-1}$. With the assumption that the UV and X-ray absorbers are the same we can determine the physical conditions and mass outflow rate of the absorbing material. We use the total hydrogen column of $N_{\text{H}} = 5 \times 10^{21} \text{ cm}^{-2}$ and the ionization parameter $U = 1.0$ from the CLOUDY modeling of the X-ray data. The distance of the absorber from the nucleus is constrained by $U = (Q/4\pi r^2 n_{\text{H}} c)^{1/2}$, where Q is the rate of ionizing photons. We used the HST data at 1339 \AA rest wavelength to scale the standard Table AGN continuum to the luminosity of MR2251–178 ($L_{\text{bol}} = 5 \times 10^{45} \text{ ergs s}^{-1}$). Integrating $L_{\nu}/(h\nu)$ over $\nu \geq 13.6\text{eV}$ gives $Q = 6h^{-2} \times 10^{54} \text{ s}^{-1}$, where h is the Hubble constant in units of $100 \text{ km s}^{-1} \text{ Mpc}^{-1}$. This puts the distance of the absorber from the nucleus at $r = 3.0 \times 10^{18} n_5^{-1/2} \text{ cm}$ (where $H_0 = 75 \text{ km s}^{-1} \text{ Mpc}^{-1}$ and n_5 is the density in units of 10^5 cm^{-3}).

The absorption extends below the continuum level (Figure 1), and so must cover a

substantial fraction of the BELR as well as the continuum source. The absorber may lie outside the BELR or it could also be cospatial with it if most of the emission is beamed from the far side of the BELR. The size of the BELR in MR2251–178 can be estimated by scaling the BELR of NGC 5548 ($L_{bol} = 5 \times 10^{44}$ ergs s $^{-1}$) by $L^{1/2}$ (Davidson & Netzer 1979; but see Kaspi et al. 2000). The distance – determined from reverberation mapping – of the BELR from the central continuum in NGC 5548 is $r \simeq 10$ light-days (Clavel et al. 1991), so the absorber in MR2251–178 must be at least ~ 32 light-days, or $r \geq 8.2 \times 10^{16}$ cm from the central source. The corresponding upper limit on the density is then $n < 1.34 \times 10^8$ cm $^{-3}$. To check the radius estimate, we specified as an input to CLOUDY the luminosity of MR2251–178 at a rest wavelength of 1339 Å, $\log(\nu L_\nu) = 43.78$, and varied the input radius to obtain the ionization parameter output previously. The radius at which $U = 1.0$ was $r = 8.76 \times 10^{16}$ cm. For a covering factor of $f = 0.1$, the column density and particle density of the absorber imply a mass of $M = 47 f_{0.1} n_5^{-1} M_\odot$. The mass outflow rate (Mathur et al. 1995) would then be $\dot{M}_{out} = 0.9 f_{0.1} M_\odot \text{ yr}^{-1}$, the same rate needed to power MR2251–178 at 10% efficiency. The rate of kinetic energy carried away in the flow is $\dot{M} v_{out}^2 / 2 = 8 \times 10^{40}$ ergs cm $^{-2}$ s $^{-1}$.

4. Conclusions

The *HST* FOS UV spectrum of MR2251–178 exhibits associated high-ionization, UV absorption lines, as predicted from models of the X-ray ionized absorber. The X-ray/UV absorber is situated outside the BELR or cospatial with it and outflowing with a line-of-sight velocity of ≈ 300 km s $^{-1}$. The mass outflow rate of $0.9 M_\odot \text{ yr}^{-1}$ for a 10% covering factor is equivalent to the accretion rate onto the nuclear black hole.

We expect future higher resolution observations will reveal each of the C IV and N V absorption lines breaking into at least two components.

The rarity of both UV and X-ray absorbers individually in radio-quiet QSOs virtually requires that the X-ray and UV absorbers are closely physically related. The consistency of the column densities obtained from both UV and X-ray data suggests the absorbers are perhaps identical. At a minimum, the X-ray absorber makes a substantial contribution to the absorption seen in the UV. Thus, the absorber in MR2251–178 satisfies both statistical as well as physical tests of our X-ray/UV absorber model.

REFERENCES

- Bergeron, J., Boksenberg, A., Dennefeld, M., & Tarenghi, M. 1983, MNRAS, 202, 125
- Clavel, J., et al. 1991, ApJ, 366, 64
- Crenshaw, D.M., Boggess, A., & Wu, C.-C. 1995, AJ, 110, 1026
- Crenshaw, D.M., & Kraemer, S.B. 1999, ApJ, 521, 572
- Crenshaw, D.M., Kraemer, S.B., Boggess, A., Maran, S.P., Mushotzky, R.F., & Wu, C.-C. 1999, ApJ, 516, 750
- Davidson, K., & Netzer, H. 1979, *Rev. Mod. Phys.*, 51, 715
- Elvis, M. 2000, ApJ, 545, 63
- Ferland, G. 1996, Univ. Kentucky, Dept. of Physics & Astronomy Internal Report
- Halpern, J.P. 1984, ApJ, 281, 90
- Hamann, F.W., Netzer, H., & Shields, J.C. 2000, ApJ, 536, 101
- Kaspi, S., Smith, P.S., Netzer, H., Maoz, D., Jannuzi, B.T., & Giveon, U. 2000, ApJ, 533, 631
- Komossa, S. 2001, A&A, in press
- Kriss, G.A. 1994, in ASP Conf. Proc. 61, Astronomical Data Analysis Software and Systems III, ed. D.R. Crabtree, R.J. Hanisch, & J. Barnes (San Francisco: ASP), 437
- Kriss, G., Espey, B.R., Krolik, J.H., Tsvetanov, Z., Zheng, W., & Davidsen, A.F. 1996, ApJ, 476, 622
- Mathews, W.G., & Ferland, G.J. 1987, ApJ, 232, 456
- Mathur, S. 1994, ApJ, 431, 75
- Mathur, S., Elvis, M., & Singh, K.P. 1995, ApJ, 455, 9
- Mathur, S., Elvis, M.S., & Wilkes, B.J. 1995, ApJ, 452, 230
- Mathur, S., Wilkes, B.J., & Aldcroft, T. 1997, ApJ, 478, 182
- Mathur, S., Wilkes, B.J., & Elvis, M. 1998, ApJ, 503, 23
- Mathur, S., Elvis, M., & Wilkes, B. 1999, ApJ, 519, 605
- Otani, C., Kii, T., & Miya, K. 1998, in IAU Symp. 188, The Hot Universe, ed. K. Koyama, S. Kitamoto, & M. Itoh (Kluwer: IAU), 436
- Ricker, G.R. et al. 1978, Nature, 271, 35
- Reynolds, C.S. 1997, MNRAS, 286, 513

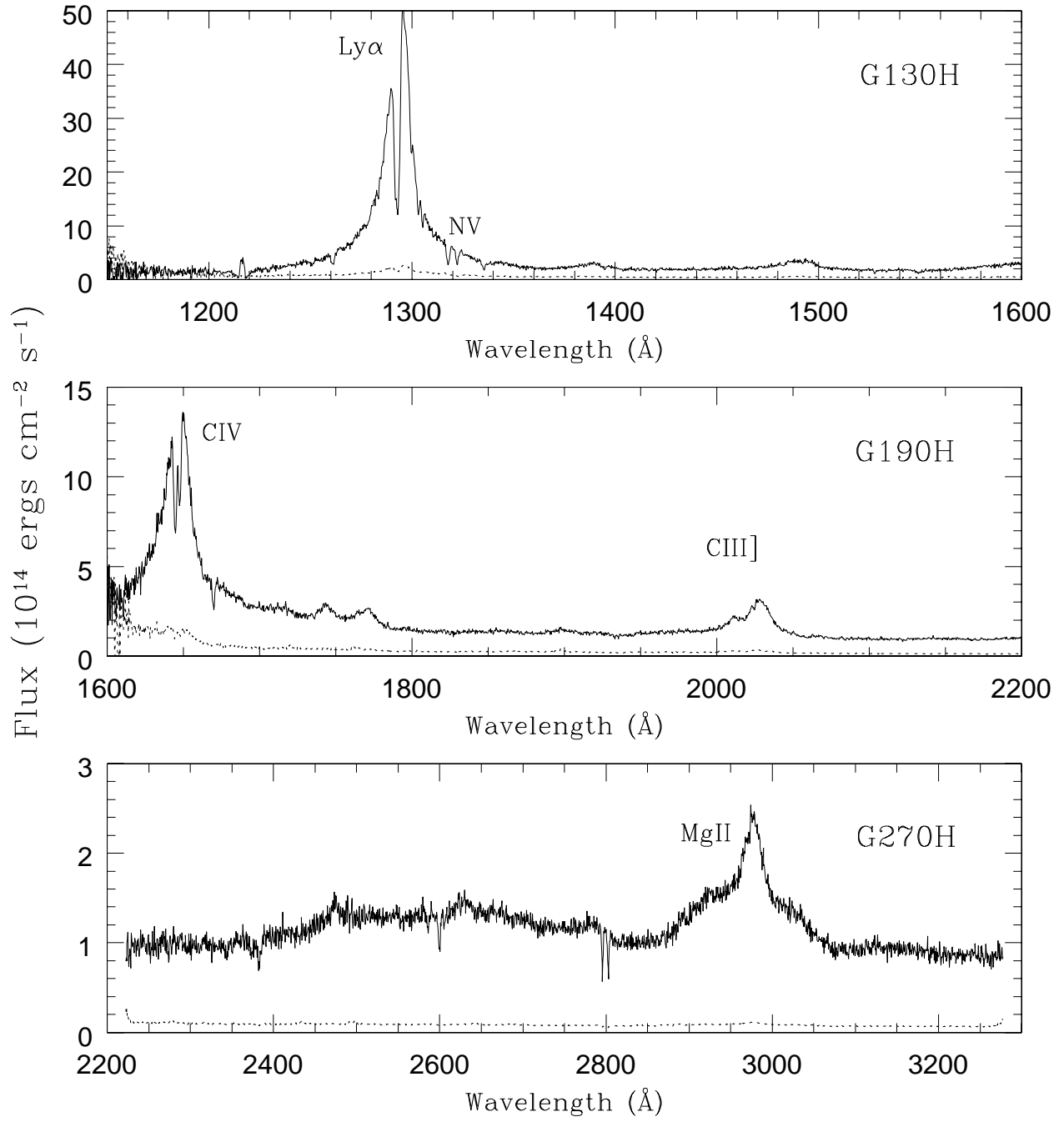
Shields, J., & Hamann, F. 1997, ApJ, 481, 752

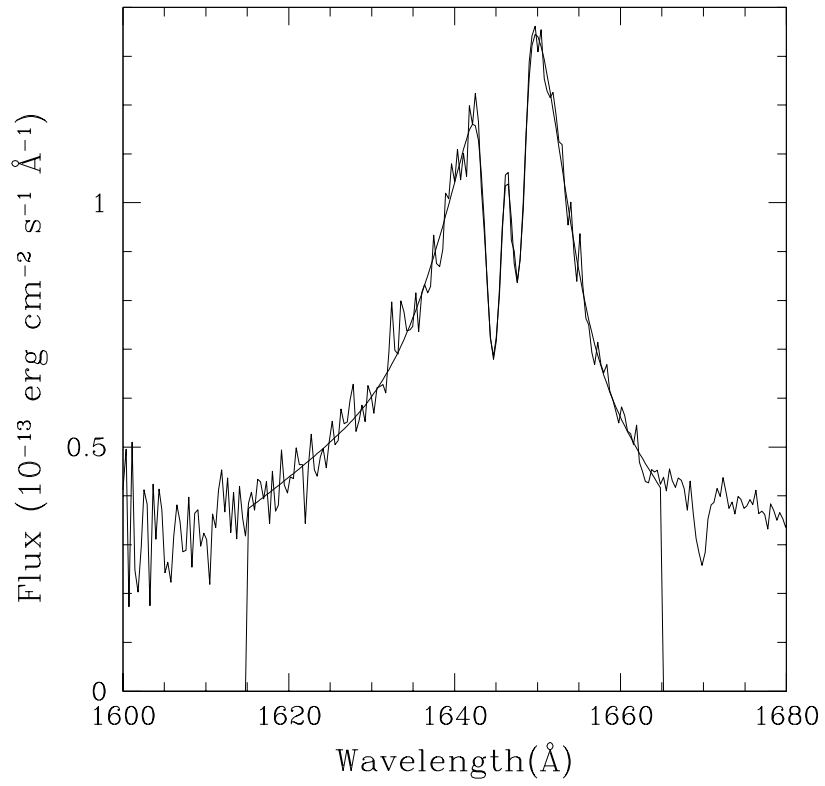
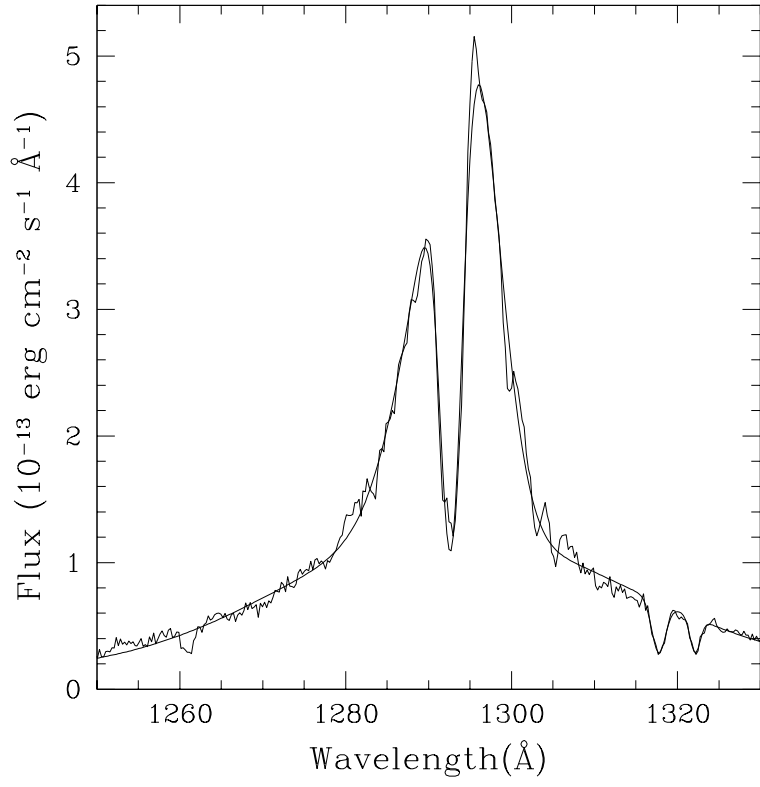
Weymann, R., Morris, S., Gray, M., & Hutchings, J. 1997, ApJ, 483, 717

Fig. 1.— *HST* spectrum of MR2251–178 showing absorption lines of Ly α , N V, and C IV. The lower line on each panel is the error spectrum.

Fig. 2.— SPECFIT fits to the absorption lines of Ly α and N V (upper panel) and C IV (lower panel). Results of the fits are shown in Table 1.

Fig. 3.— SPECFIT fit to the *HST-STIS* spectrum of the Ly α absorption line of MR2251–178. Results of the fit are shown in Table 1.





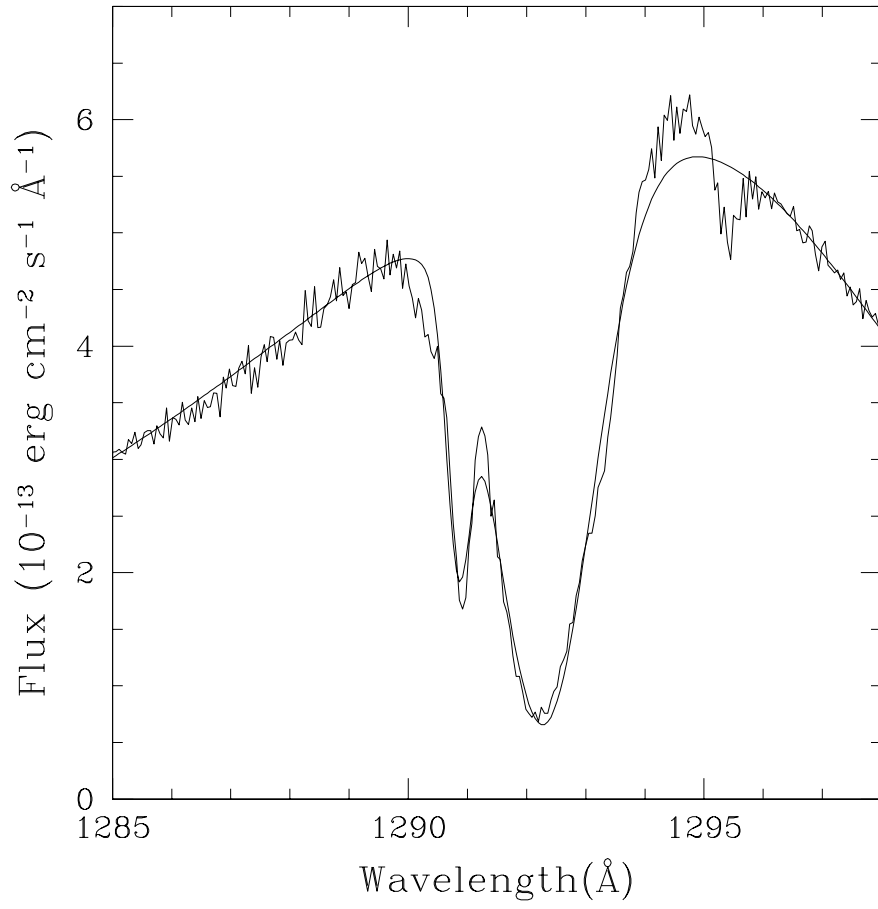


Table 1. **Absorption Line Parameters**

Line	Instrument	λ_{obs} (Å)	z	EW ^a (Å)		FWHM (km s ⁻¹)		N_{ion} (cm ⁻²)	
				SPLIT	SPECFIT	SPLIT	SPECFIT	Observed ^b	Predicted ^c
Ly α 1215.7	FOS-G130H	1292.6	0.0630	2.22	2.52 \pm 0.08	694	754 \pm 23	>(3.8 - 4.4) $\times 10^{14}$	8.4 $\times 10^{14}$
Ly α 1215.7	STIS-G140M	1290.9	0.0619	–	0.26 \pm 0.01	–	108 \pm 37	(6.4 $\times 10^{13}$) ^d	
Ly α 1215.7	STIS-G140M	1292.3	0.0630	–	1.90 \pm 0.01	–	475 \pm 24	(6.4 $\times 10^{14}$) ^d	
C IV1548.2	FOS-G190H	1644.7	0.0623	1.07	1.09 \pm 0.08	434	410 \pm 25	>(6 - 7) $\times 10^{14}$	1.6 $\times 10^{13}$
C IV1550.8	FOS-G190H	1647.6	0.0624	0.64	0.80 \pm 0.07	399	363 \pm 25		
N V1238.8	FOS-G130H	1317.8	0.0637	1.02	1.14 \pm 0.11	382	444 \pm 51	>(10 - 11) $\times 10^{14}$	1.6 $\times 10^{14}$
N V1242.8	FOS-G130H	1322.2	0.0638	0.61	0.71 \pm 0.10	304	325 \pm 57		

^aRest-frame EW. SPLIT error estimates are 40% on Ly α and CIV, 10% on NV.

^bThe FOS values are lower limits from the linear part of the C.O.G. Two numbers correspond to SPLIT and SPECFIT values.

^cPrediction from photoionization code CLOUDY using "Table AGN" input continuum.

^dCurve-of growth measurement.